ESDA2010-24900

POOR-CONTRAST PARTICLE IMAGE PROCESSING IN MICRO SCALE MIXING

F. Gökhan Ergin*
Scientific Instrumentation

Bo Beltoft Watz
Research & Development

Kaspars Erglis
Department of Physics

Andrejs Cebers
Department of Physics

Dantec Dynamics A/S
Tonsbakken 16-18
Skovlunde, 2740 Denmark

University of Latvia
8 Zellu Str.
Riga, 1002 Latvia

ABSTRACT

Particle image velocimetry (PIV) often employs the cross-correlation function to identify average particle displacement in an interrogation window. The quality of correlation peak has a strong dependence on the signal-to-noise ratio (SNR), or contrast of the particle images. In fact, variable-contrast particle images are not uncommon in the PIV community: Strong light sheet intensity variations, wall reflections, multiple scattering in densely-seeded regions and two-phase flow applications are likely sources of local contrast variations. In this paper, we choose an image pair obtained in a micro-scale mixing experiment with severe local contrast gradients. In regions where image contrast is sufficiently poor, the noise peaks cast a shadow on the true correlation peak, producing erroneous velocity vectors. This work aims to demonstrate that two image pre-processing techniques – local contrast normalization and Difference of Gaussian (DoG) filter – improve the correlation results significantly in poor-contrast regions.

Keywords: Particle image velocimetry, image processing, labyrinthine instability, local contrast normalization, difference of Gaussian filter.

INTRODUCTION

Particle image velocimetry has matured over a quarter century and is now an established tool in fluid diagnostics. The history and general principles of the technique can be found in two review articles [1, 2]. The development of the technique has been tremendous due to relentless advances in laser, detector, and CPU processor technology: In 25 years, the technique evolved from the manual construction of a 2-component velocity field from a double-exposed particle image on a single photographic paper, to digital storage and computation of 3-component velocity fields in liter-sized volumes in a time resolved fashion. Along the way, several other sub-techniques and names, such as Digital-PIV, Micro-PIV, Nano-PIV, Holo-PIV, Stereo-PIV, Tomo-PIV have been introduced to describe certain variations of the technique. In this paper we restrict our discussions to a monoscopic, planar, two-component velocity field measurement in a micro-scale mixing experiment.

Current monoscopic PIV standard is the recording of two individual time-separated particle images on a double-frame planar photo-detector array (CCD or CMOS) illuminated by a double-cavity pulsed laser. The images are then divided into smaller interrogation regions where the cross-correlation map for the two consecutive recordings is calculated. Assuming that the source density, time separation, interrogation window size and the image density are optimized, the height of the correlation peak depends strongly on the signal-to-noise ratio of the particle images. The pixel value distribution of an image depends on the scattering mode used in the acquisition: Side-scatter reflection (or refraction for transparent seeding) will often result in an image with bright particles on a dark background. Alternatively, forward-scatter illumination, often used in shadow imaging and transmission microscopy applications will result in images with dark particles (shadows) on a bright background. In either case, a good contrast between the particle and the background will produce a better correlation peak, and provide an accurate displacement measurement.

Contrast variations are not uncommon among raw PIV images and might occur due to several reasons. The first reason

---

*Corresponding author; Gokhan.Ergin@dantecdynamics.com

is the light source: An ideal laser beam is circular, has an axis-symmetric Gaussian intensity distribution in the near-, middle-, and far-field with an M^2 value close to unity. However, the real beam emitted from the laser aperture is often far from ideal in all aspects. If these deviations are severe, a laser sheet with undesirable intensity variations is obtained when the beam is stretched using sheet optics. Another reason for the local contrast variations is the existence of a boundary. Wall reflections and densely seeded flows can easily produce saturated pixels in the detector, and in the limit, the sensor might be irreversibly damaged. Similar examples are the existence of larger particles and/or bubbles among the smaller seeding particles. A third reason is the existence of several liquids with different absorption coefficients, such as in a mixing experiment. In this work, the authors choose an image pair obtained in a micro-scale mixing experiment with severe local contrast gradients (Figure 1).
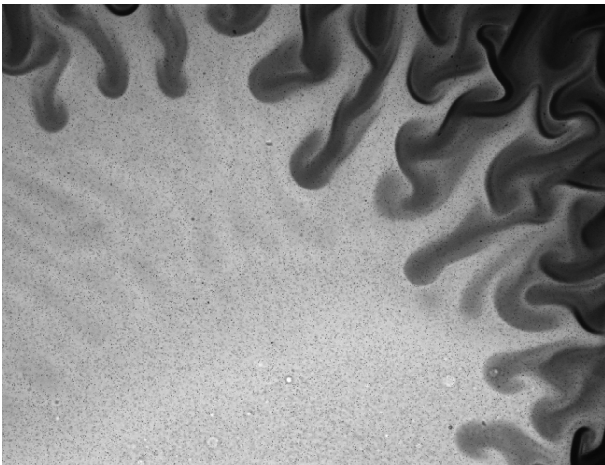

Figure 1. Particle image of the magnetic mixing experiment, displaying the labyrinthine instability between the magnetic fluid (dark) and solvent (bright region).

Mixing enhancement using magnetic forces has been a popular technique in micro-scales, as the flows tend to remain laminar in such scales and the mixing of two miscible fluids is dominated by molecular diffusion. In a magnetic micro-convection experiment two miscible fluids, one doped with magnetic particles, are placed side-by-side in a Hele-Shaw cell, representing a step-like concentration gradient. Under the action of a homogenous magnetic field normal to the concentration gradient, the magnetic fluid is forced into the solvent manifesting a characteristic labyrinthine instability at the interface. Once formed, this finger-like pattern smears out in time due to molecular diffusion (Figure 1). This instability is analogous to the Rayleigh-Taylor instability resulting from the density differences under the action of gravitational field.

The labyrinthine instability has been subject to extensive theoretical and experimental research. Maiorov & Cebers [3] provide a mathematical formulation assuming even perturbations and two-dimensional motion of the interface. Reference 3 also provides the first experimental evidence of "finger-like" and "tongue-like" structures at the interface, with observations on the characteristic spatial period of the pattern. Cebers [4] performs a linear stability analysis, introduces a magneto-viscous number, which is the ratio of magnetic to viscous forces, and illustrates that the fingering phenomenon is observed when the magnetic field strength exceeds a threshold value. Igonin & Cebers [5] provide a comprehensive review on the subject with an extensive list of references: they generalize the problem by considering a miscible magnetic fluid pair and perform a linear stability analysis, with analytical results for the sharp interface and numerical results for the diffuse concentration distribution. Derec et al. [6] observe "long fingers" under the effect of milder magnetic fields and "splitting fingers" under the effect of stronger magnetic fields in an experiment validating the observations of Maiorov & Cebers [3]. The parametric study reveals that time; cell separation distance and magnetic field strength individually affect the characteristic wavelength of the fingers. The motivation of this work is to provide the first quantitative data, i.e. the velocity field associated with the labyrinthine instability.

EXPERIMENTAL SETUP

The experiments are performed using a micro-PIV system manufactured by Dantec Dynamics (Figure 2). The system consists of a HiPerformance inverted fluorescent microscope, HiSense MkII high-quantum efficiency, double-frame CCD camera with 12-bit image resolution, MicroStrobe pulsed LED illumination device; system controller and advanced synchronization unit with 12.5 ns time resolution. The system controller is equipped with a Dual Xeon 2.33 GHz Quad core processor, 4GB RAM running Windows XP operating system and Dynamic Studio v2.10.86 software platform for dedicated synchronization, hardware control, database management, image processing library and PIV analyses.
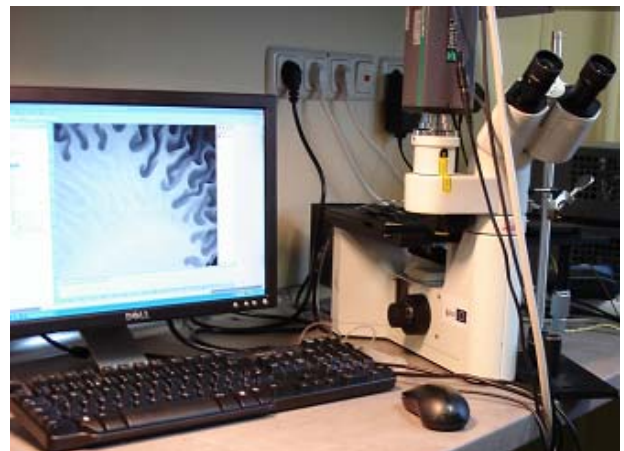

Figure 2. Dantec Dynamics MicroPIV system.

The Hele-Shaw cell was prepared using two cover glasses separated with 127 µm-thick *Parafilm*. The channels for fluids and air was cut in *Parafilm* and cured by heating after assembly. The pure solvent is prepared by mixing 100 µl of fluorescent particles (2% solid) in 10 ml of distilled water. The colloidal solution of magnetic nanoparticles is prepared by adding fluorescent micro-particles in the magnetic fluid. The water based magnetic fluid was produced from γ-Fe_2O_3 magnetic particles with a nominal size of 10 nm. This is achieved by precipitating anionic magnetite from aqueous solution of Fe^{2+} and Fe^{3+} chlorides using ammonium hydroxide. A few drops of magnetic fluid were introduced on the right side of cell using a micropipette, until the capillary forces filled one half of the cell with magnetic fluid. Then, few drops of pure solvent were introduced from the other side until the pure solvent came in contact with the magnetic fluid. The fluorescent seeding particles are carboxilate-modified microspheres with 1 µm diameter. The particles are Nile-red fluorescent (between 535-575 nm) and are quite suitable for high-resolution MicroPIV applications. The particles are introduced both in the magnetic fluid and the solvent as light scatterers. No attempt was made to differentiate the particles in the two regions during PIV analysis.
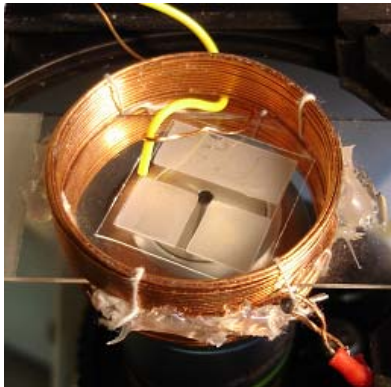

Figure 3. The Hele-Shaw cell placed in the center of the electromagnet.

The Hele-Shaw cell was placed in the center of an electro-magnet, a 38-turn-coil of 0.7-mm-diameter wire (Figure 3). A current of 2A from *Kepco* BOP 20-10M power supply produced a magnetic field strength of 1.8 mT in the central part of the coil. The field was applied before pure solvent mixed with magnetic fluid.

The second frame of the raw image pair acquired with this setup is shown in Figure 1. In this acquisition, the field of view (FOV) is 1.6 mm x 1.2 mm using a 10x objective. The trigger rate is set to 3 Hz; time between pulses is 81,68 ms, first and second pulse duration is 450µs, and 550 µs respectively. The dark region is the colloidal solution of magnetic nanoparticles and fluorescent particles. The bright region is the pure solvent containing 1-µm-diameter fluorescent particles, which are

visible as shadows. The image pair is acquired several seconds after the colloidal solution and solvent are brought in contact.

RESULTS

Without prior image processing, conventional advanced PIV algorithms fail in the darker regions where the image contrast is poor. The vector field obtained using an adaptive correlation algorithm with 2 refinement steps, 2 pass per step, 32-pixel-wide square interrogation windows, and 50% overlap is shown in Figure 4. No Fourier window, filter, peak validation or local smoothing is applied in order to have a basic comparison of vectors in the FOV. It is necessary to perform image pre-processing to obtain valid vectors in the regions shaded by the magnetic nanoparticles. Same pre-processing scheme is applied to both frames of the particle image pair.
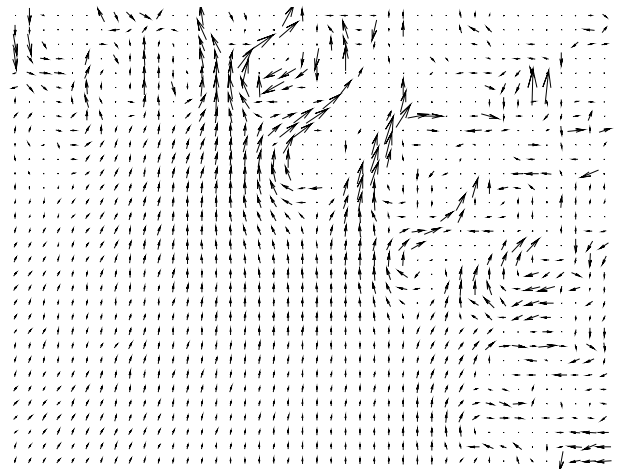

Figure 4. Multi-step, multi-pass adaptive correlation results performed on the raw image pair. Every second vector is displayed.

Contrast normalization [7] (also called pixel value normalization) is a fairly common image enhancement technique, simply rescaling all pixel values in an image to exploit the full range of values supported. For a typical 12-bit image this could be described as:

$$p_{new} = 4095 \frac{p_{old} - p_{min}}{p_{max} - p_{min}}$$

where p_{old} and p_{new} describe old and new pixel values, while p_{min} and p_{max} describe the smallest and highest pixel values present in the original image. After contrast normalization the darkest and brightest pixel values are guaranteed to be 0 and 4095 respectively. Local contrast normalization is similar; the only difference is that p_{min} and p_{max} are not derived from the full image, but from a local neighborhood of pixels in the vicinity of the pixel being scaled. This is accomplished by means of the morphological operations of opening and closing, where the neighborhood is determined by the size and shape of the structuring element. In this example a round structuring element was used, which is 15 pixels in diameter. To reduce the

influence of noise a 3x3 median filter was applied prior to the morphological operations. In addition to this, a 9x9 median filter is applied repeatedly as an edge-preserving smoothing filter (Figure 5).
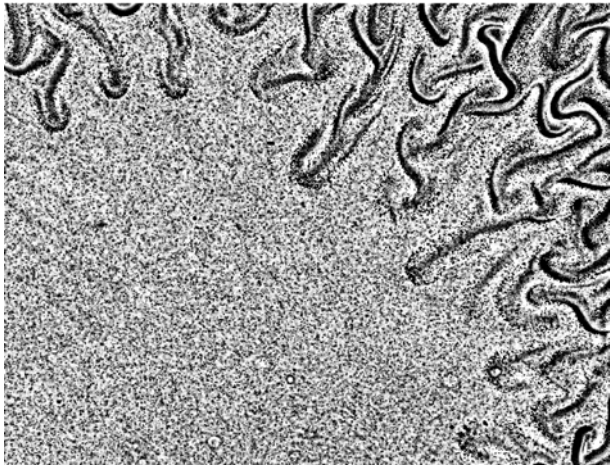

Figure 5. Processed particle image in Figure 1, after the application of local contrast normalization.

The processed images still contain some noise after the local contrast normalization operation. For example, the dark-strips in Figure 5 appear on the regions of steep pixel value gradients in the raw image in Figure 1, as a result of the fixed, 15-pixel-diameter structuring element. More sophisticated edge-detection algorithms could be used to make an adaptive-diameter structure, but this is not in the scope of this work. It is necessary to apply a high-pass filter to highlight particle images. The preferred filter used here is a so-called, Difference of Gaussian (DoG) filter, implemented by convolving the image with a 7x7 kernel shown in Table 1, and then dividing by a common divisor; 636.

-1	-6	-15	-20	-15	-6	-1
-6	-20	-26	-24	-26	-20	-6
-15	-26	31	84	31	-26	-15
-20	-24	84	176	84	-24	-20
-15	-26	31	84	31	-26	-15
-6	-20	-26	-24	-26	-20	-6
-1	-6	-15	-20	-15	-6	-1

Table 1. Coefficients of the 7x7 convolution kernel for the DoG filter.

The DoG filter is in fact the difference between two images, each derived by applying different Gaussian filters to the same original image. The convolution kernel shown in Table 1 corresponds to a 5x5 Gaussian minus a 7x7 Gaussian. The processed particle image after the contrast normalization and DoG filter operations is shown in Figure 6.

Figure 6. Processed particle image in Figure 1, after the application of local contrast normalization and DoG filter.

The vector field obtained from the processed images using the same adaptive correlation algorithm is shown in Figure 7. Every second vector is displayed in both directions and, again, no window, filter and smoothing function is applied. However, a mild local median validation scheme with 63% acceptance factor is applied in a 3x3 neighborhood to replace the spurious vectors (1% of total). The corresponding vorticity map is also displayed with warm colors indicating positive, cold colors indicating negative and the green color indicating zero vorticity.
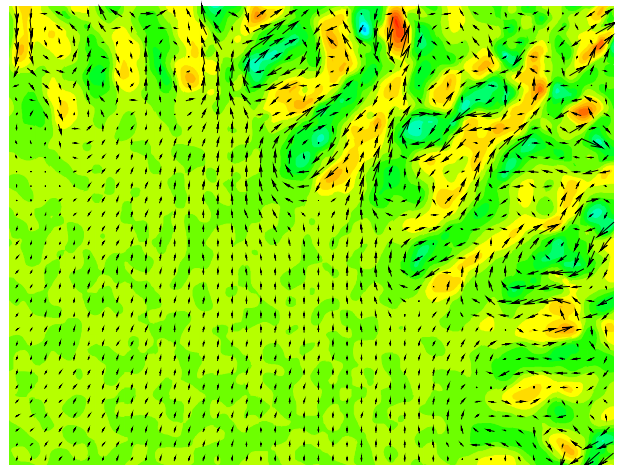

Figure 7. Multi-step, multi-pass adaptive correlation results performed on the processed image pair. Every second vector is displayed overlaid on the vorticity field.

It is clear from Figure 7 that the proposed image pre-processing scheme has enabled the calculation of valid vectors in the dark regions of the raw particle image. In order to have a validity check for the algorithm, the difference of vector maps with and without image processing can be used. The difference vector map shows small deviations in the lower left corner of

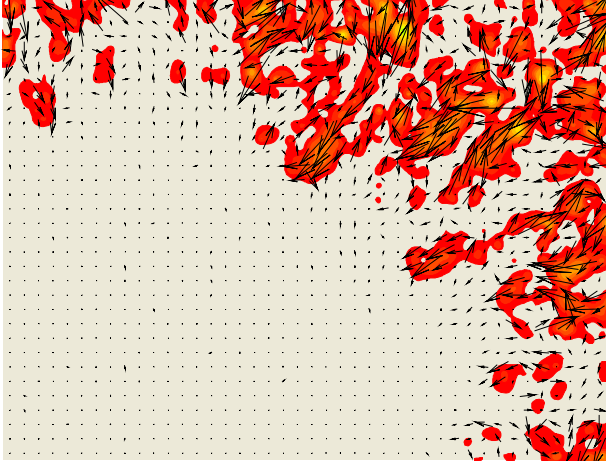the FOV and large deviations in the rest (Figure 8), as expected.

Figure 8. Difference between vector fields obtained with and without image processing. Every second vector is displayed overlaid on the scalar vector length.

CONCLUSIONS AND FUTURE WORK

The potential of image processing functions in obtaining vector maps from variable-contrast particle images is illustrated. In this particular work, local contrast normalization (or pixel value normalization) and DoG filter is used to obtain clean particle images for a magneto-hydrodynamic mixing application. This experiment provides the first quantitative MicroPIV velocity field measurement for the labyrinthine instability. Future work includes a parametric investigation of this instability with quantitative velocity data and the temporal evolution of the interface. The techniques applied here are not claimed to be universal, i.e. they may or may not be applicable to other image pairs obtained in other applications. More sophisticated algorithms will be developed to have an adaptive technique that may tackle many different types of contrast variations. Combined with an advanced edge detection capability, these algorithms may be applicable to flame front investigations in combustion diagnostics.

REFERENCES

[1] Adrian, R. J., 2005, "Twenty years of particle image velocimetry", *Experiments in Fluids*, Vol. **39**, pp. 159-169.

[2] Willert, C., 2009, "Recounting twenty years of digital PIV, its origins and current trends", *Proceedings of 8th Int. Symposium on Particle Image Velocimetry – PIV09*, Melbourne, Australia (August 2009)

[3] Mairov, M. M. and Tsebers A. O., 1983, "Magnetic microconvection on the diffusion front of ferroparticles", *Magnetohydrodynamics*, Vol. **19**, pp. 376.

[4] Cebers A., 1997, "Stability of diffusion fronts of magnetic particles in porous media (Hele-Shaw cell) under the action of external magnetic field", *Magnetohydrodynamics*, Vol. **33**, pp. 48.

[5] Igonin, M. and Cebers A., 2003, "Labyrinthine instability of miscible magnetic fluids", *Physics of Fluids*, Vol. **15**, No. 6, pp. 1734-1744.

[6] Derec, C., Boltenhagen, P., Neveu, S., and Bacri J.-C., 2008, "Magnetic instability between miscible fluids in a Hele-Shaw cell", *Magnetohydrodynamics*, Vol. **44**, No. 2, pp. 135-142.

[7] Westerweel, J., 1993, "Digital Particle Image Velocimetry – Theory and Application", *Delft University Press*.